Article

Failure of ceramics due to impact loading

Wing Cheng*, K.C. Jin**, and Shigeru Itoh***

Failure of ceramics to impact loading was investigated deterministically using quasi-static finite element analysis and theory of fracture mechanics. It was demonstrated that multiple cracks were initiated, however, not all cracks would propagate. Mode II fracture dominated the fracture conoid within the contact zone while Mode I dominated outside the contact zone. From the analyses, the force versus penetration curve was derived and applied to a ballistic design program with which the ballistic performance of ceramic panels could be determined.

1. Introduction

The high compressive strength of ceramics has made it a potential material for lightweight armor systems. Ceramics has been used in conventional armor as well as hybrid armor systems. The subject of this study was the case of a ductile and sharp-nosed projectile which may be defeated by plastic deformation of the tip resulting in a larger contact surface when impacting a ceramic target.

Quasi-static finite element analysis of an elastic-plastic body contact was used to approximate the phenomenon when a ductile sharp-nosed projectile impacted a ceramic penal. The extent of the plastic deformation in the projectile (from sharp to blunt) was predicted by the analysis, however, the amount of any defeated material was not separated in this static analysis since the failure of this material is a dynamic process and was not considered in this study and reserved for future research.

The purpose of the analysis reported here was two-folded. First, it was to obtain a better understanding of the failure mechanisms of ceramics when impacted by a ductile but sharp-nosed projectile. It was assumed that this relationship is similar to the static indentation force relationship in principle. Such relationship was incorporated into a design program [1] formulated based on an equivalent energy dissipated system [2,3].

Once the projectile was defeated, it resulted in a larger contact zone as well as many fracture conoids. Moreover, each fracture conoid propagated at a different velocity (dynamically) and a different time (i.e. inner conoid occurs earlier). The fracture process is very complex in nature and is dynamic. To understand this phenomenon, a series of quasi-static finite element analyses of multiple-crack systems were employed using techniques derived from fracture mechanics. A brittle fracture mechanics-based progressive failure model was developed to predict initiation, location, and direction as well as propagation of multiple cracks. It was found that Mode II dominates the fracture conoids inside the contact zone, and Mode I dominates the fracture conoid (neglecting wave effect, only one major conoid) outside the contact zone. Therefore, if the propagation speed through the thickness of the outside fracture conoid is faster than the defeated projectile, the fracture conoid may be separated from the armor (complete penetration).

2. Materials

The ceramic used in this study is alumina

Received : May 17, 2002
Accepted : Semtember 6, 2002
*MechComp Inc.
Sunnyvale, California, USA
**AC Engineering
West Lafayette, Indiana, USA
***Shock wave and Condensed Matter Research Center
Kumamoto University
Kumamoto, JAPAN

porcelain (90-95% Al_2O_3). The material constants are [4]

Young's Modulus (Et)	$=53 \times 10^6$ psi
Poisson's Ratio (n)	$=0.3$
Density (d)	$=3.0 \times 10^{-4}$ lb-sec^2/in^4
Compressive Strength (Yc)	$=5.8 \times 10^6$ psi
Tensile Strength (Xt)	$=4.35 \times 10^4$ psi

In addition to these properties, the density of the steel projectile is 0.0007 lb-sec^2/in^4. The Young's modulus of the projectile is 30 x 10^6 psi; its radius and length is 0.4" and 0.9", respectively.

3. Ceramic failure mechanisms

Experiments show that the ceramic-fracture conoids are relatively independent of impact velocity because the same conoids always occur over the impact velocity range of interest [5,6]. One conclusion which can be drawn is that the 5.8 x 10^6 psi (40 GPA) compressive yield strength of the alumina ceramic (Al_2O_3) is sufficient to destroy the tip of the projectile in the first 10 μs [7]. This allows a greater surface area to contact the armor and therefore the projectile energy can be more rapidly dispersed, which would be possible with armor-grade steels, but not aluminum or mild steel. A simplification is possible if the force-defeated material length relation can be found. In order to study the relation, an axisymmetric finite element model is analyzed with the ABAQUS general purpose finite element program. The analysis considered a circular ceramic that is pushed transversely at the center by a sharp indentor; see Fig. 1. The ceramic and the indentor are both modeled as deformable bodies. The axisymmetric finite element model is demonstrated in Fig. 1.

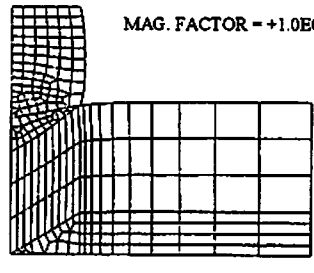

Fig. 1 Final deformed geometry of a static indentation process

The radius and thickness of the ceramic is 1.8" and 0.9", respectively. The indentor is given a motion in the -y direction by prescribing a specific displacement at the tail of the indentor. The analysis, being nonlinear, is conducted in an incremental manner. Thus, in the following analyses, the analyses are performed until the pointed indentor becomes flat (fully contact with the armor).

Under the pressing action of the indentor, both the indentor and ceramics deformed progressively and as shown in Fig. 1, the indentor experienced a tremendoous deformation (from sharp to blunt). At that instant, the maximum principal stress are all compressive. Since the compressive strength of the alumina oxide (Al_2O_3) is 5.8×10^6, no compressive damage occurs in the ceramics. However, there is compressive damage at the impact region of the indentor as the stresses exceed its compressive stength (1.5×10^5 psi). In other words, it is natural to see the indentor being defeated (breaking off the point) when pushed into the ceramics. Unfortunately, the amount of the defeated material is not reflected from this quasi-static analysis. An alternative approach similar to [1] is to find the force-displacement relation of this energy dissipating system. The contact force versus indentation depth has been recorded based on the above analyses. The results are shown in Fig. 2. A polynomial curve fitting is also shown in the picture. This curve can be directly utilized as the 1st nonlinear spring in the design program [1].

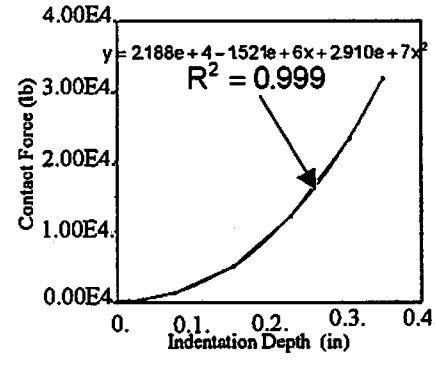

Fig. 2 Contact force versus indentation depth for pure ceramics.

4. Multiple crack systems

Knowledge of the stresses which develop in the ceramic is important in understanding the onset and propagation of the brittle fracture to be evaluated. A simple constitutive model that was used to describe the fracture (initiation and propagation) of the ceramic incorporated the following assumptions and principles: (1) fracture is initiated on surfaces; (2) the criterion for fracture initiation was a maximum principal stress greater than 43.5 ksi of tension, the crack direction is associated with the principal stress direction; (3) the strain energy release rate (G) associated with the new (longer) crack geometry must be checked. If the new G for the newly formed crack exceeds the original G (initial shorter crack), crack propagation was possible. This crack propagation was allowed until G fell below the original G (fracture toughness); (4) if the projectile has been defeated before fractures pass through the ceramic, more circumferential fractures will be generated due to more contact area; (5) the multiple circumferential cracks will compete with each other based on the driving force of each crack; (6) a complete penetration occurs when a certain conoid underneath the projectile drops out (fracture passes through the thickness). Requirements (4)-(5) have to be checked each time before (6).

The initial finite element model (without cracks) and the rigid pointed projectile is used to simulate the initial contact without defeating the projectile tip as demonstrated in Fig. 3. Since the ceramic is usually strong in compression and weak in tension, it is very easy to observe tensile cracks in ceramics.

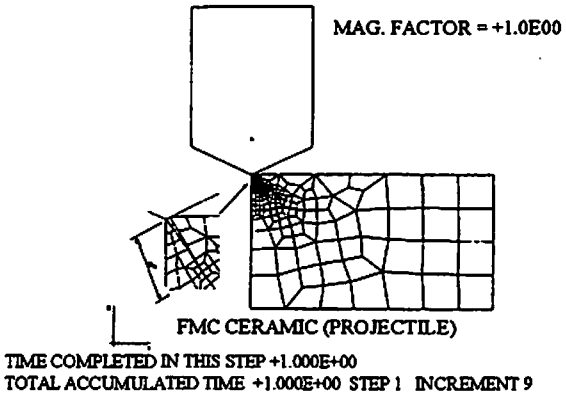

Fig. 3 Deformed geometry of ceramics with a crack size (a_o) at the contact site.

Analysis results indicated that cracks would be initiated at the contact site. The displacement of the projectile (0.002") is too small and can be neglected (i.e. the cracks will initiate at the instant the projectile and the ceramics are in contact). The direction of these cracks is between 0° – 40°. In reality, many cracks (ranging from 0° in the center line to a specific angle away from the center line) will exist at various orientations due to the pointed projectile and the brittle nature of ceramics.

Figure 3 shows that a fracture conoid develops at the contact site with an orientation 30° to the right of the center line, as obtained from the analysis. The initial crack length is a_o, the calculated total G is 0.0143 lb-in/in^2 at projectile displacement equal to 0.002". The crack closure technique [2] was used to calculate the G_I and G_{II}. A subroutine was developed as a post-processing step to calculate the strain energy release rate G_i. A longer crack size (a_1) was used for the same projectile displacement (0.002"), the new G for this newly formed crack is 0.011 lb-in/in^2, which is smaller than the original G (0.0143 lb-in/in^2) when the crack size is a_o. Therefore, the crack would not propagate when the projectile doesn't push further. A stable crack growth is seen at this stage.

The actual fracture of the neighboring zone is governed by the crack propagation velocity and time elapsed (i.e. dynamic process). A systematic quasi-static analysis is used to understand the mechanism behind the dynamic process. The advantage of the ceramic is its hardness properties. It can destroy the projectile tip in the first 10 μs. This allows a greater surface to contact the target and therefore the projectile energy can be more rapidly dispersed. Moreover, the process is a stable crack growth stage as stated above. Therefore, it is more likely to have a greater contact area between the projectile and the target.

A different projectile (rigid) shape is used to simulate the projectile being defeated after a certain period. In order to satisfy the criterion of crack initiation (i.e. the maximum tensile stress should be greater than 43.5 ksi), the projectile has to displace 0.005" thus additional cracks are initiated at those critical areas. This value (0.005") is still

small when compared to the thickness (0.9") of the target, so it can be neglected (i.e. the additional crack will initiate on the edge of the projectile (contact site), so an additional crack will initiate at the edge. It is concluded that during the projectile defeating process, more contact area is being generated (i.e. more circumferential cracks at the edges occurred when the projectile being flattened out). The crack orientation is obtained from the principal stress direction contours of a number of elements in the vicinity of the contact edge. The angle (orientation) is determined to be around 40° to the right of the center line. Therefore, there are many cracks ranging from 0° to 40° underneath the contact area.

In order to simplify the multiple crack propagation system, only two cracks (inner and outer) are demonstrated to simulate the different fracture behaviors (modes). They are shown in Figure 4. The initial crack lengths of both cracks are a_0, the calculated total G for the inner and outer cracks are 0.232 lb-in/in^2 and 2 lb-in/in^2, respectively. It should be noted that G_I (Mode I) of both cracks are zero (by crack closure method), which means only Mode II fracture is seen underneath the contact area. Moreover, the fracture toughness (G_c) of Mode II is usually one order of magnitude higher than Mode I for most materials, therefore it is more difficult to see Mode II type crack propagation in a real situation.

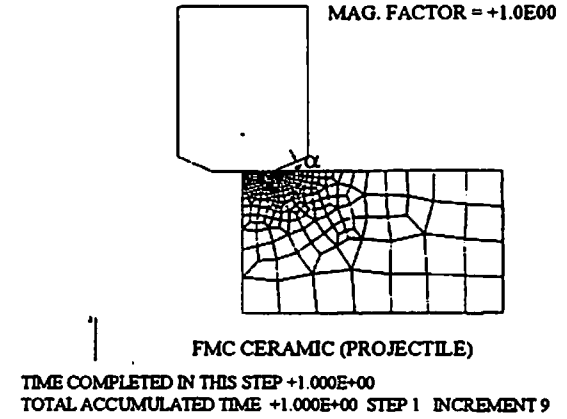

Fig. 4 Deformed geometry of ceramics with a center crack (1) and a crack at contact site (2)

However, since approximated values of fracture toughness for Modes I and II are known, only qualitative phenomena can be extracted from these analyses. That is, the G of the outer crack (2 lb-in/in^2) is one order higher than the inner one (0.232 lb-in/in^2). Therefore, if crack propagation is possible, the outer crack will propagate faster. Also, Mode I fracture has some relation to the angle α of the projectile shape. This means when α is greater than a specific angle, the opening component of the crack tip exists, which results in a nonzero G_I. This phenomenon will be discussed again later when the sidewall of the projectile contacts the target.

It is assumed that the projectile continues to be defeated before fracture passes through the ceramics. More evidence is required to verify that the fracture is actually under stable crack growth procedure. If the outer crack is located just inside the contact area (i.e., more projectile material being defeated), the total G is dropped from 2 lb-in/in^2 to 0.248 lb-in/in^2. This indicates that a stable crack growth is observed when a crack is inside the contact region. Moreover, the G_I (open mode) is zero due to the stresses within the contact area are all compression. When considerably different projectile shape is used for simulating continuous defeat of the projectile, the calculated total G continues dropping to 0.139 lb-in/in^2.

The largest contact area occurs when the contact edge is the sidewall of the projectile. The maximum principal stress contours are illustrated in Fig. 9. The critical stresses are located on the edge of the projectile (contact site) and back surface (bending crack). The bending crack (radial crack) will try to propagate upward. In addition, the crack orientation at the contact site (edge) is determined from the principal stress direction contour of six elements around the contact site. The angle (orientation) is found to be about 60° to the right of the center line. The shear component plays an important role of positioning the cracks on the free surfaces. The orientation is 45° in a pure shear case. Therefore, in the graphical ballistic design program, the orientation is simplified and assumed to be 45°.

There are four major crack systems representing the brittle fracture phenomena of ceramics as shown in Fig. 5. They are categorized

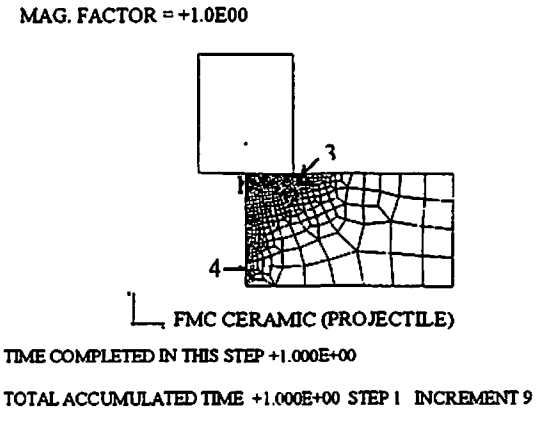

Fig. 5 Deformed geometry of ceramics with four major crack system (a short outside crack).

into: (1) the center crack; (2) cracks underneath the contact area; (3) the outside major crack; and (4) the bending crack (See Figure 5). The initial crack size of (2) is assumed longer than (1) because of the previous conclusion (i.e., the G of the outer crack (2) is one order higher than the inner one (1), so the outside crack will propagate longer than the inside one even if the crack growth is stable).

The calculated G (G_I & G_{II}) at a projectile

Table 1 Calculated strain energy release rate of cracks (1) – (4) at projectile displacement of 0.005" (short outside crack)

Strain Energy Release Rate	Center (1)	Under Projectile (2)	Outside Projectile (3)	Bending (4)
G_I	0.	0.	0.	0
G_{II}	0.345	10.22	9.36	0.03
$G(G_I+G_{II})$	0.345	10.22	9.36	0.03

displacement of 0.005" is given in Table 1. It is obvious that the strain energy release rate of cracks (1) and (4) are much smaller than cracks (2) and (3). Therefore, it is reasonable to assume that the cracks (1) and (4) would not propagate at all. Moreover, if the crack systems (2) propagate, they will propagate in Mode II manner. It is interesting to note that the outside major crack (3) has a large G_I (16.7 lb-in/in^2), which is caused by the crack contacting the side wall (α= 90°) of the projectile. The crack opening (tensile) stress concentration results around the outside major crack tip. However, the inside crack tips are dominated by compression. Therefore, it is more likely to see the outside fracture (Mode I) propagating much faster than the inner fractures (Mode II).

The outside major crack is extended to a longer size (larger than cracks (2)) to simulate the faster crack propagation. The strain energy release rate at the projectile displacement equals 0.005" for all crack systems which are presented in Table 2. It is noted that the strain energy release rate (G_I &

Table 2 Calculated strain energy release rate of cracks (1) – (4) at projectile displacement of 0.005" (medium outside Crack)

Strain Energy Release Rate	Center (1)	Under Projectile (2)	Outside Projectile (3)	Bending (4)
G_I	0.	0.	2.5	0
G_{II}	0.35	5.74	1.54	0.035
$G(G_I+G_{II})$	0.35	5.74	4.04	0.035

G_{II}) of cracks (2) and (3) have been reduced because the boundary conditions have changed (i.e, a longer outside major crack). Therefore, both crack systems propagate in a stable manner. This can be verified by continuing to move the projectile downward. The calculated G (G_I & G_{II}) at the projectile displacement equals 0.006" and is provided in Tables 3. The strain energy release rates of both cracks systems ((2) and (3)) show a

Table 3 Calculated strain energy release rate of cracks (1) – (4) at projectile displacement of 0.006" (medium outside crack)

Strain Energy Release Rate	Center (1)	Under Projectile (2)	Outside Projectile (3)	Bending (4)
G_I	0.	0.	27.64	0
G_{II}	0.45	8.77	18.64	0.045
$G(G_I+G_{II})$	0.45	8.77	46.28	0.045

tremendous increase, but the maximum projectile displacement (0.01") is still very small when compared to the target thickness (0.9"). In addition, the G_I (opening mode) of the outside major crack increases very rapidly (i.e, it will try to propagate in an unstable Mode I manner under a

specific projectile displacement). The stress concentration behavior of the cracks has emphasized this most important unstable Mode I crack propagation.

Next, a much longer outside major crack is illustrated in Fig. 6 to simulate the unstable Mode I crack propagation. The calculated strain energy release rate (G_I & G_{II}) at a specific projectile

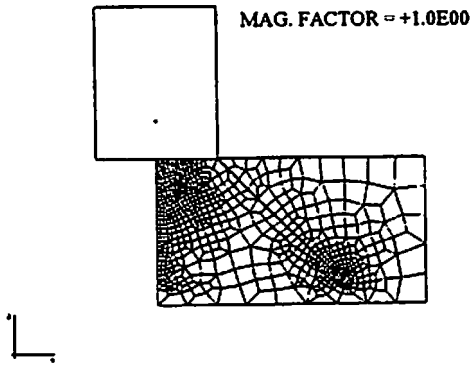

Fig. 6 Deformed geometry of ceramics with four major crack system (a long outside crack).

Table 4 Calculated strain energy release rate of cracks (1) – (4) at projectile displacement of 0.006" (long outside crack)

Strain Energy Release Rate	Center (1)	Under Projectile (2)	Outside Projectile (3)	Bending (4)
G_I	0.	0.	115.4	0
G_{II}	0.113	1.026	85.6	0.126
$G(G_I+G_{II})$	0.113	1.026	201.0	0.126

displacement (0.006") is shown in Table 4. Comparing to Table 3, it is clear that the outside major crack (3) is under an unstable crack growth process (G increases), but cracks (2) are in a stable growth procedure (G decreases). A very high tensile stress concentration is confined to the outside major crack tip. Since the G_I (115.4 lb-in/in^2) driving force is so high for the crack (3) tip, it is very likely to pass through the target thickness resulting in a drop out of the fracture conoid. This is due to unstable crack growth (Mode I) of the outside major crack.

Finally, the multiple crack systems can be drawn schematically in Fig. 7 which shows the crack propagation phenomenon in this multiple crack system as follows: (the inner cracks are always propagate slower (shorter) than the outer ones). Also, the contact force is reduced when the outside major crack extends to a larger length, See Fig. 8.

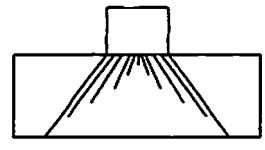

Fig. 7 Schematics of a multiple crack system.

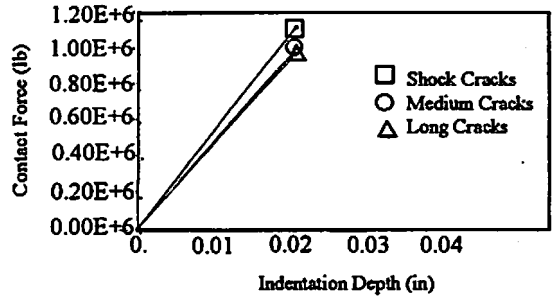

Fig. 8 Contact force versus indentation depth with different outside crack lengths.

5. Other impact damage modes

The most general features of projectile impact damage (circumferential cracks) on ceramic targets are described in the previous sections. Moreover, (1) bending cracks (radial direction) will generate from the back face; and (2) compression-type cracks (Mises stress) will introduce under the contact area if there is a back up plate underneath the ceramic armor. These two other distinct forms of dominant fracture are radial (bending) and compression (Mises stress) cracks. Radial cracks are less important (not propagating because the circumferential cracks are dominant in the previous case). Radial cracks in the bottom surface tend to become dominant if the ceramics are thin enough. The maximum stresses are located in the center of the bottom surface and oriented along the radial and hoop directions (σ_{rr} and σ_{qq}). The cracks caused by these two stresses all propagate in the radial direction and through the thickness of the target. In addition, the circumferential cracks will occur at the contact site. The materials

that are strong in compression are usually weak in tension. This has led to the development of composite targets in which a ceramic face plate is backed up by a material that can resist failure from tensile stresses. This results in the projectile penetrating the ceramics slowly, and the materials underneath the contact zone have fractured due to squeezing action between the projectile and back up plate. Mises stress is used to evaluate this type of compression failure.

Two tensile (circumferential) cracks outside the

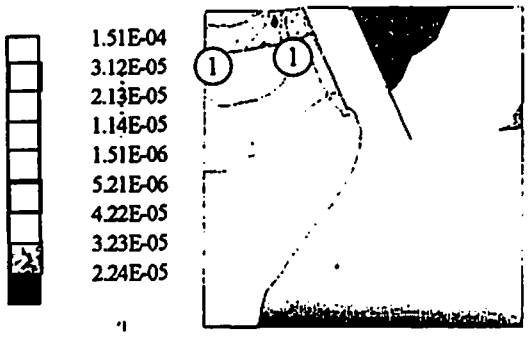

Fig. 9 Maximum principal stress distribution of ceramics with outside major cracks and a compression crack (symbol①-①).

contact area and a compression crack (symbol ①-① in Fig. 9) is illustrated in Fig. 9. The Mises-type failure can be derived from the critical Mises region of the Mises stress distribution of this multiple crack system. The contact force versus indentation depth relation of different cracking system is plotted in Fig. 10. Therefore, the actual contact force will switch from the curve (no

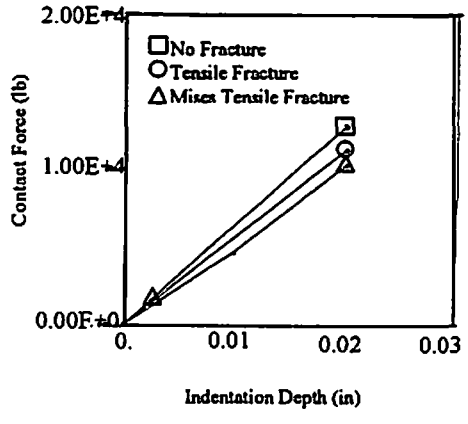

Fig. 10 Contact force versus indentation depth of ceramics with tensile and Mises failures.

fracture) to the one (tensile fracture), and so forth. If we slowly deactivate the material properties in the critical Mises area, then the curve (Mises and tensile fracture) as shown in Fig. 10 will start to level off and may continue dropping as more materials are deactivated. Future research should be concentrated in this area.

6. A dual panel example

Although the application of the analysis of separate target plates is straightforward for determining the penetration characteristics [1], i.e., the model is applied to each plate separately in successive order so that the residual velocity of the projectile after perforating the first layer, becomes the initial impact velocity for the second layer. It is interesting to perform an example to predict the ballistic performance of a kevlar/ ceramic (Al_2O_3) dual panel in the design program.

The initial velocity of the FSP projectile is 6,217 ft/sec (74.600 in/sec). Its length and diameter is 1.077" and 0.877", respectively. A taper region (projectile tip) is extended from length equals 0.913" to the tip. Also, the diameter of the tip is 0.407". The first panel is a 1.75" thick kevlar laminate, the second panel is a 1.5" (Al_2O_3) ceramic panel. For the first panel, punching shear damage is the only damage mode as in [1], the punching shear strength (S*) is equal to 40 ksi. The final penetration of the first panel is demonstrated schematically in Fig. 11. The residual velocity of the first panel is about 4,167 ft/sec (50000 in/sec), which is the impact velocity of the second panel. The resulting reduction in kinetic energy of the first panel is over 50%. It took 29 micro-seconds

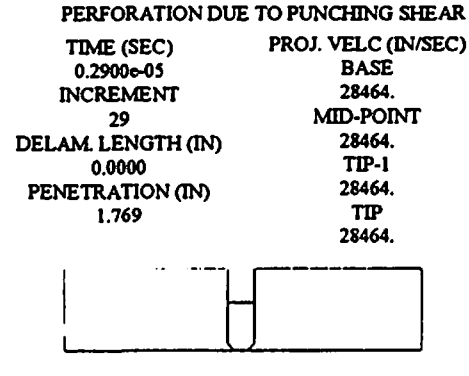

Fig. 11 Final penetration stage at 1st (Kevlar) panel – at 29 μsec.

to penetrate the first panel.

The exit velocity from the Kevlar panel was used as the initial impact velocity to the ceramics. The defeated projectile and target failure at the final stage is illustrated in Fig. 12. The ultimate fracture was assumed to initiate and propagate through the

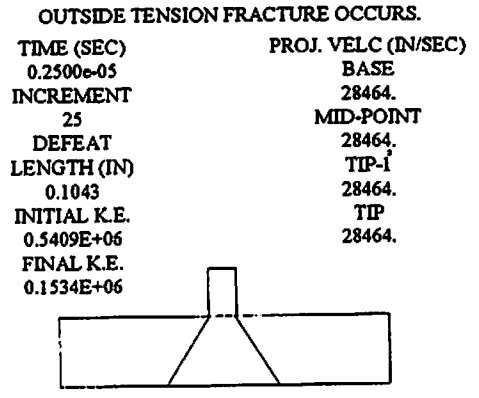

Fig. 12 Final fracture stage at 2nd (Ceramic) panel – at 2.5 μsec.

thickness when the projectile starts to bounce back. The final residual velocity is 2,371 ft/sec (28,460 in/sec). It is concluded that the projectile tip is destroyed within 2.5 micro-seconds. The rate of projectile energy loss increases as the surface area of the projectile in contact with the target increases. This is due to the high compressible yield strength of the ceramics. The target (ceramics) absorbs approximately 70% of the projectile energy, which can be easily calculated from the residual kinetic energy.

7. Conclusions

The current investigation demonstrated the complexity of ceramic failure mechanics and models. Several important conclusions can be drawn from this study. (1) The projectile tip has been defeated before penetrating into the ceramic (due to high compressive strength of ceramics). (2) A brittle fracture mechanics based progressive failure model was developed to predict initiation location and direction as well as propagation of multiple cracking systems. (3) The fractures inside the contact zone are Mode II dominant; but the fractures outside the contact zone are mostly Mode I. Mode I cracks propagate much faster than Mode II cracks. (4) Bending cracks are mostly initiated on the bottom surface and propagate in the radial direction. Compression cracks occur between the projectile and the ceramics, if there is a backup plate.

Finally, a ballistic design program previously developed for composites targets was modified to accommodate the above mechanisms and was applied to a pure ceramic armor system. The resulting program delivered an extremely fast and relatively accurate simulation of elapsed time and projectile residual velocity, and is useful for sizing of armor systems.

8. Acknowledgements

The authors would like to thank the Management of Corporate Technology Center for their financial support and encouragement of this R & D Project The content of this paper first appeared in the Proceedings of Dynamic Response of Structures to High-Energy Excitations Symposium, 1991 ASME Winter Annual Meeting, The Applied Mechanics Division and The Pressure Vessels and Piping Division, December 1-6, 1991, AMD-Vol. 127/PVP-Vol. 225, edited by T.L. Geers and Y.S. Shin.

References

1) Cheng, W., Langlie, S.; 1990; "A simplified analytical model for impact/penetration process in thick fiber-reinforced composites", Proceedings of the 2nd International Conference on Computer-aided Design in Composite Material technology, Brussels, Belgium.
2) Cheng, W., Langle, S.,; 1996,; " A Composite Model for High Velocity Impact - Implementation of a Simplified Delamination Criterion", Proceedings on the 67th Shock & Vibration Symposium, Volume II, Monterey, CA, U.S.A.
3) Cheng, W., Langle, S.,; 1996,; " Partitioning of delamination and bending during impact penetration of thick composites ", To be published.
4) Kingery, W.D, Bowen, H.K., Uhlmann, D.R.; 1976; Introduction to Ceramics, 2nd Edition, John Wiley & Sons, Table 15.1.
5) Wilkins, M.L., Fline, C.F., Honodel, C.A.; 1969;

"Fourth progress report on light armor program", Report UCRL-50694, Lawrence Livermore Radiation Laboratory, University of California.
6) Wilkins, M.L.,; 1980; "Computer Simulation of Penetration Phenomena", Ballistic Materials and Penetration Mechanics, Elsevier, 1980.
7) Laible, R.C.; 1980; "Ceramic Composite Armor", Ballistic Materials and Penetration Mechanics, Elsevier, 1980.